An infusible biologically active adhesive for chemotherapy-related heart failure in elderly rats

Jialu Yao [a,1], Junlang Li [c,1], Dashuai Zhu [b,1], Yuan Li [b,c], Panagiotis Tasoudis [d], Shuo Liu [b], Xuan Mei [e], Kristen Popowski [b], Thomas G. Caranasos [e], Haipeng Wang [a], Mingzhu Xu [a], Tingbo Jiang [a,**], Kan Shen [f,***], Hongxia Li [a,****], Ke Huang [b,*]

[a] Department of Cardiology, The First Affiliated Hospital of Soochow University, Suzhou, 215000, China
[b] Department of Molecular Biomedical Sciences, NC State University, Raleigh, NC, USA
[c] Joint Department of Biomedical Engineering, University of North Carolina Chapel Hill and North Carolina State University, Raleigh, NC, USA
[d] Division of Cardiothoracic Surgery, University of North Carolina at Chapel Hill, Chapel Hill, NC, USA
[e] Division of Engineering in Medicine, Department of Medicine, Brigham and Women's Hospital, Harvard Medical School, Cambridge, MA, 02139, USA
[f] Department of Critical Care Medicine, Shanghai University of Medicine and Health Sciences Affiliated Zhoupu Hospital, Shanghai, China

ARTICLE INFO

ABSTRACT

Chemotherapy-induced cardiotoxicity with subsequent heart failure (HF) is a major cause of morbidity and mortality in cancer survivors worldwide. Chemotherapy-induced HF is exceptionally challenging as it generally manifests in patients who are typically not eligible for left ventricular device implantation or heart transplantation. To explore alternative treatment strategies for cancer survivors suffering from chemotherapy-induced HF, we developed a minimally invasive infusible cardiac stromal cell secretomes adhesive (MISA) that could be delivered locally through an endoscope-guided intrapericardial injection. To mimic the typical clinical presentation of chemotherapy-induced HF in elder patients, we established an aged rat model in which restrictive cardiomyopathy with sequential HF was induced *via* consecutive doxorubicin injections. In vitro, we prove that MISA not only enhanced cardiomyocytes proliferation potency and viability, but also inhibited their apoptosis. In vivo, we prove that MISA improved the ventricular contractility indexes and led to beneficial effects on histological and structural features of restrictive cardiomyopathy via promoting cardiomyocyte proliferation, angiogenesis, and mitochondrial respiration. Additionally, we also evaluated the safety and feasibility of MISA intrapericardial delivery in a healthy porcine model with an intact immune system. In general, our data indicates that MISA has a strong potential for translation into large animal models and ultimately clinical applications for chemotherapy-induced HF prior to the final option of heart transplantation.

1. Introduction

Advancements in anticancer therapies have offered improvements in the survival of cancer patients [1]. However, contemporary data indicate that one out of ten cancer survivors ultimately passes away due to cardiovascular-related etiologies and 80% of these mortalities is attributable solely to heart diseases [2]. Heart disease in cancer survivors commonly arises de novo or is exaggerated by the cardiotoxic side effects of the chemotherapeutic agents [3,4]. The pathophysiology behind chemotherapy-induced heart disease lies in the cardiomyocyte death or

damage complications caused by chemo-induced reactive oxygen species and abnormal mitochondria functions [3]. This heart problem presents in cancer survivors, whose quality of life is already affected by their primary disease, and that makes it an even more sensitive healthcare issue [5]. To date, heart transplantation remains the only conclusive treatment option for HF [6,7]. However, cancer survivors are typically not deemed eligible for this option due to their past medical history and their frail baseline status. For these reasons, we sought to explore deliverable therapeutics for cancer survivors with chemotherapy-induced HF.

Advancements in cell-based therapeutics are credited to mitigate the adverse heart remodeling, reduce scar tissue formation after myocardial injury, and repair (or regenerate) viable myocardial tissue through paracrine mechanisms [8–11]. However, the clinical application of cell therapy has been hindered by challenges such as targeting, retention, efficacy, and immune reactions. To address these issues, we have previously developed microparticles (synCSCs) that encapsulate a concentrated secretome derived from cardiac stromal cells for the treatment of ischemic heart injury [12]. This acellular product is easily obtained by encapsulating the concentrated CSC secretome in Poly(lactic-co-glycolic acid) (PLGA), an FDA-approved biodegradable and biocompatible polymer. In order to enhance local delivery efficiency and facilitate translation to clinical practice, we have designed a clinically feasible, easy-to-store, off-the-shelf, and cell-free cardiac patch to deliver synCSCs to the epicardial surface of a diseased heart [13]. However, the previous delivery method for this synCSC cardiac patch necessitates an open-chest surgery to place the patch directly onto the heart. In this study, we designed a mini-invasive infusible version of synCSCs adhesive (MISA) to overcome the challenges associated with the "Open-Chest" delivery route.

The effectiveness of synCSCs (synthetic cardiac stem cells) for ischemic cardiac repair has been demonstrated, but further research is necessary to assess their potential benefits for chemotherapy-induced HF. Despite distinct causes and mechanisms, there are notable similarities between chemotherapy-induced HF and ischemic heart injury, particularly in their impact on the heart and the development of HF. For example, chemotherapeutic agents like doxorubicin, daunorubicin, idarubicin, and epirubicin can lead to cardiomyopathy through various complex mechanisms. Recent studies suggest that these agents cause direct mitochondrial injury, generate reactive oxidative species (ROS), and free ferric cations, ultimately resulting in oxidative stress and triggering cardiomyocyte ferroptosis. In an ischemia/reperfusion heart, however, ROS also plays a significant role in tissue damage during the reperfusion phase. The primary source of ROS generation during IR injury is the degradation of ATP, leading to the production of hypoxanthine during the ischemic phase. Upon reperfusion, an influx of molecular oxygen catalyzes xanthine oxidase, converting hypoxanthine into uric acid and releasing highly reactive superoxide anions (O_2^-). Despite the demonstrated effectiveness of synCSCs in ischemic cardiac repair, their potential benefits for chemotherapy-induced HF warrant further investigation.

In this study, we investigated the effectiveness of synCSC in addressing chemotherapy-induced HF by injecting MISA into the pericardial cavity of an aged rat heart with chemotherapy-induced HF. MISA offered a better synCSC delivery route that was required for future clinical translation, especially for cancer patients who are typically unable to tolerate aggressive procedures [13]. To mimic the clinical picture of cancer survivors with chemotherapy-HF, we established an aged rat model with restrictive cardiomyopathy *via* consecutive doxorubicin injections [14]. Taken together, MISA was ultimately developed with the potential to revolutionize the current treatment for chemotherapy-induced HF.

2. Results

2.1. Fabrication of MISA

The fabrication process and injection of MISA are illustrated in Fig. 1A using a previously described method [1,2]. According to our histology results, the decellularization step was efficient (Fig. 1B). The ECM gel was created to deliver synCSCs that are enveloped inside. To prevent the leakage of injected gel from the injection site after the needle was withdrawn, we added fibrinogen by mixing the ECM hydrogel with a commercially available fibrinogen solution (1:1) to promote rapid gelation of our solution after injecting it concomitantly with thrombin. SynCSCs (8×10^6/ml) were embedded into a solubilized ECM-fibrinogen solution to create the semifinal product of MISA, named "Semi-MISA". A double-lumen syringe was separately loaded with Semi-MISA and thrombin solution (10 mg/ml) to facilitate synchronous delivery into the pericardial space of the heart. The combination of Semi-MISA and thrombin generated our final product, aptly named "MISA". The morphological features of MISA were visualized in cryo-scanning electron microscopy (SEM) (Fig. 1C). We also assessed the decellularized cardiac ECM structure, gelatinized 3D structure of empty gel (MISA without synCSCs), MISA, and its key component synCSC, through SEM imaging. SynCSCs were observed to be efficiently and uniformly embedded in the adhesive (Fig. 1D). These data suggested the success of using ECM-fibrinogen solution to create Semi-MISA, which was then combined with thrombin to produce the final MISA.

2.2. Regenerative potency of MISA in vitro

The regenerative potential of synCSCs has been reported previously [12,13]. To further confirm the result, we performed Immunocytochemistry on neonatal rat cardiomyocyte culture plates after 3 days of co-culturing equal amounts of phosphate-buffered saline (PBS), empty gel (MISA without synCSCs), synCSCs alone, and MISA, respectively. The ki67 expression of the cardiomyocytes was significantly increased in the MISA and synCSCs group compared to the others (Fig. 2A and B). To confirm and validate the proliferation of cardiomyocytes, the expression of pH3 (phosphorylated Histone 3) (Fig. 2C and D) and Aurora B (Fig. 2E and F) were further evaluated in the nuclei, both of which demonstrated a higher proliferative state when co-cultured with synCSC and MISA compared to the other two groups. Remarkably, the MISA and synCSC groups showed similar proliferation. Live/Dead assay (Figs. S1A–S1B) suggested that the number of cardiomyocytes in the MISA group was substantially higher than in the other groups. An extended cytotoxic study was performed via TUNEL assay (Figs. S1C and S1D). The cardiomyocytes co-cultured with synCSC and MISA had significantly lower TUNEL$^+$ expression rates than those of the other two groups. Together, the results from our *in vitro* co-culture system and all the aforementioned assays demonstrated the regenerative effect of MISA on cardiomyocytes, laying the groundwork for the following *in vivo* studies.

2.3. MISA in the chemotherapy-HF in aged rats

2.3.1. Animal model creation and study design

To test the therapeutic potency of MISA *in vivo*, we induced HF in aged (1-year-old) SD rats by injecting four doses of doxorubicin (DOX) intraperitoneally within 2 weeks, aiming to mimic aged patients who develop HF after chemotherapy [14,15]. Four months after the first DOX dose, the successful establishment of the restrictive type of HF model was confirmed via echocardiography with a reduced left ventricle ejection fraction (LVEF) and left ventricle fractional shortening (LVFS) when compared to sham-controlled animals (Figs. S2A and S2B). Following that, the treatments were administered through intrapericardial (iPC) injection [16]. Briefly, the animal models were allocated into four distinct groups: (a) negative control animals that received HF induction only, (b) empty gel animals that received iPC
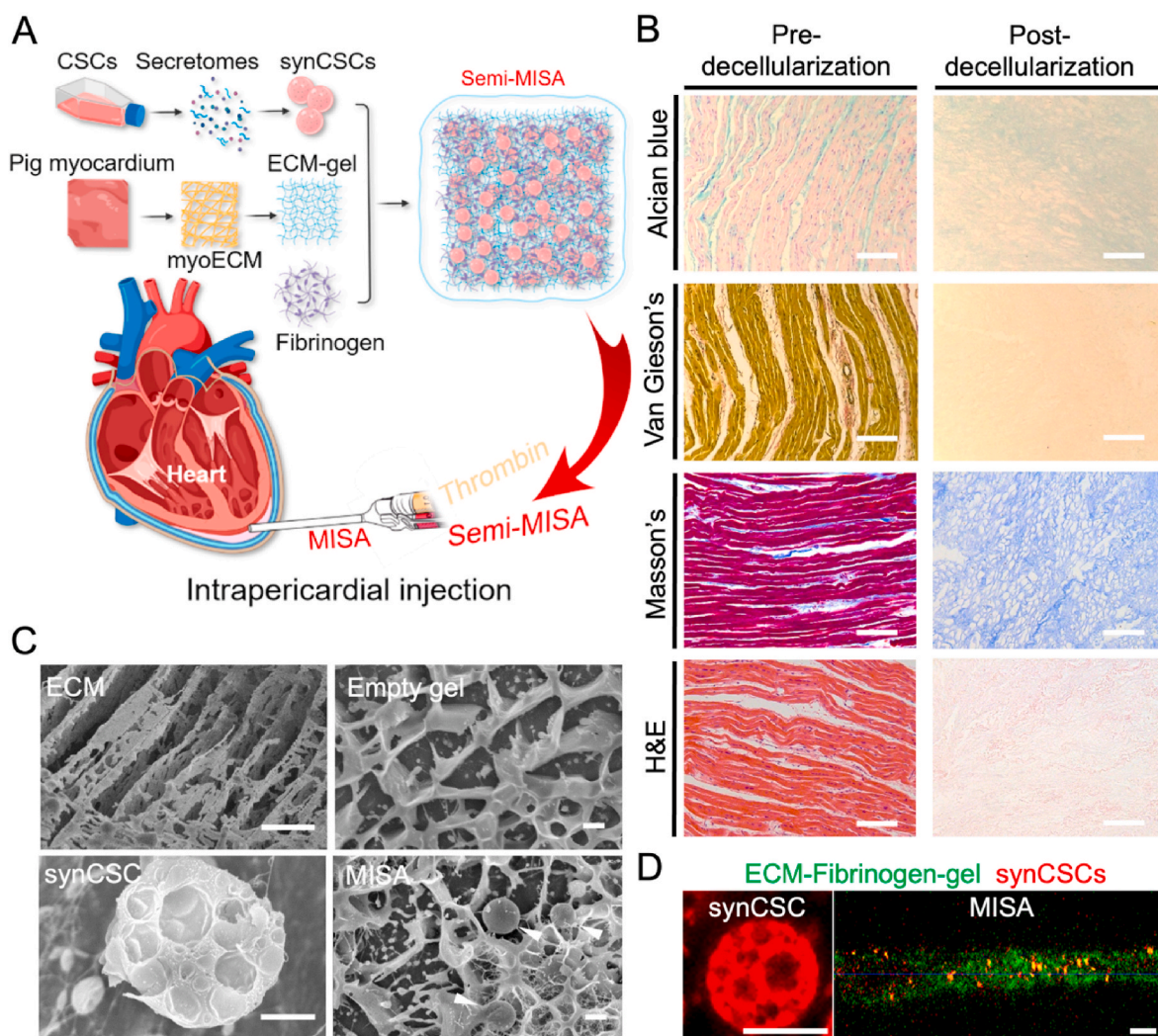
Fig. 1. Fabrication and characterization of MISA. A. Schematic showing the fabrication process of MISA and intrapericardial injection. **B.** Histological comparison of pig myocardium pre- and post-decellularization, including Alcian blue, Van Gieson's, Masson's trichrome, and H&E staining. Scale bars = 100 μm. **C.** Representative SEM images showing the decellularized ECM (Scale bar = 10 μm), empty gel (ECM-fibrinogen-gel, Scale bar = 1 μm), synCSC (Scale bar = 1 μm), and MISA (Scale bar = 1 μm). The arrowheads indicated synCSCs loaded within the MISA structure. **D.** Representative confocal images of synCSCs and 3D confocal images of the synCSC's distribution in MISA. synCSCs were labeled by DiD dye (red), Collagen-1 was used to label ECM-Fibrinogen gel (green). Scale bar (synCSC) = 2 μm. Scale bar (MISA) = 25 μm.

injection of MISA without synCSCs , (c) synCSC-only animals that received iPC injection of synCSCs suspended in PBS, and finally (d) the MISA animals that received iPC injection of MISA. All animals were euthanized 28 days after MISA administration, and all hearts were harvested for histological analysis (Fig. 3A).

2.3.2. Heart morphometry and fibrotic changes after MISA treatment

The heart morphometry changes were visualized through Masson's trichrome staining. The results indicated that MISA reduced the total interstitial fibrosis area of the chemotherapy-injured hearts compared to the synCSCs-only group as well as the other control groups (Fig. 3B and C). MISA was also associated with a reduced left ventricular (LV) wall thickness compared to the control groups (Fig. 3C). Together, MISA reduced the interstitial fibrotic area that was induced by DOX administration and facilitated the maintenance of a healthier heart morphology.

2.3.3. MISA offers beneficial effects on cardiac pumping function

In terms of functional benefits, echocardiography was performed before MISA administration as a baseline level and before the animals were euthanized on day 28 as an endpoint. LVEF and LVFS at baseline

(Day 0) did not show significant differences among all groups, outlining the uniformity of the cardiac function and the degree of initial injury prior to MISA application (Fig. 3D–F and S3A). Four weeks after treatment (Day 28), the models that had received MISA injection displayed an improvement in LVEFs. Although the LVFS was comparable among all groups, the LVIDs and LVIDd were higher in the MISA-treated group, which implied that heart compliance was better than that of the control groups (Figs. S3A–C). It should be clarified that the fact that LVIDd was found lower after DOX application confirmed the successful establishment of a restrictive HF model. The LVESV and LVEDV showed neglectable differences within the study groups (Fig. 3E–F). We hypothesized that these results might be attributed to a potential decrease in interstitial fibrosis following MISA administration. To examine this hypothesis, we utilized wheat germ agglutinin (WGA) staining (Fig. S4A) to quantify the cross-sectional area of the interstitial fibrosis per high power field (Fig. S4B). Our results indicated that MISA reduced the interstitial fibrosis in the HF heart. Of note, we observed some therapeutic effects in the synCSC-only group as well as in the empty gel-control; however, embedding of synCSCs in the MISA seemed to have significantly amplified the therapeutic effects.
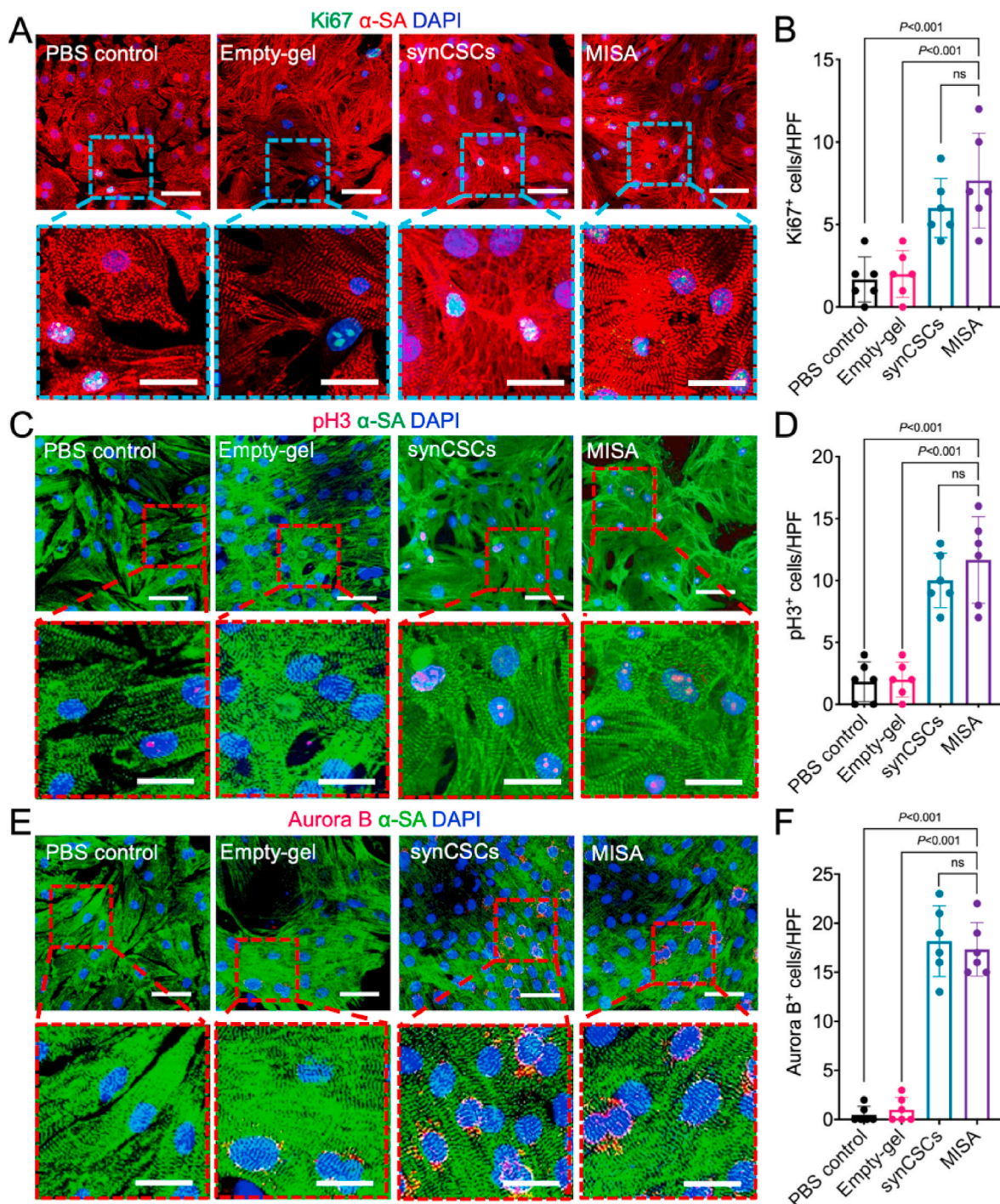
Fig. 2. Proliferative effects of MISA on cardiomyocytes *in vitro*. A. Representative images of immunofluorescence staining of Ki67 marker in neonatal rat cardiomyocytes (NRCMs) in different groups. Ki67 (green) was used to label proliferative cells among cardiomyocytes. Sarcomeric α-actinin (α-SA) (red) is an indicator of cardiomyocytes. Nuclei were labeled with DAPI (blue). Lower images show higher-magnification views of the boxed areas in the upper images. Scale bars, lower magnification, 50 μm; higher magnification, 25 μm. **B.** Quantitative analysis of cells in (**A**), n = 6 in each group. **C.** Representative images of immunofluorescence staining of pH3 marker in NRCMs in different groups. pH3 (red) was used to label proliferative cells among cardiomyocytes. α-SA (green) is an indicator of cardiomyocytes. Nuclei were labeled with DAPI (blue). Lower images show higher-magnification views of the boxed areas in the upper images. Scale bars, lower magnification, 50 μm; higher magnification, 25 μm. **D.** Quantitative analysis of cells in (**C**), n = 6 in each group. **E.** Representative images of immunofluorescence staining of Aurora B marker in NRCMs in different groups. Aurora B (red) was used to label proliferative cells among cardiomyocytes. α-SA (green) is an indicator of cardiomyocytes. Nuclei were labeled with DAPI (blue). Lower images show higher-magnification views of the boxed areas in the upper images. Scale bars, lower magnification, 50 μm; higher magnification, 25 μm. **F.** Quantitative analysis of cells in (**E**), n = 6 in each group.
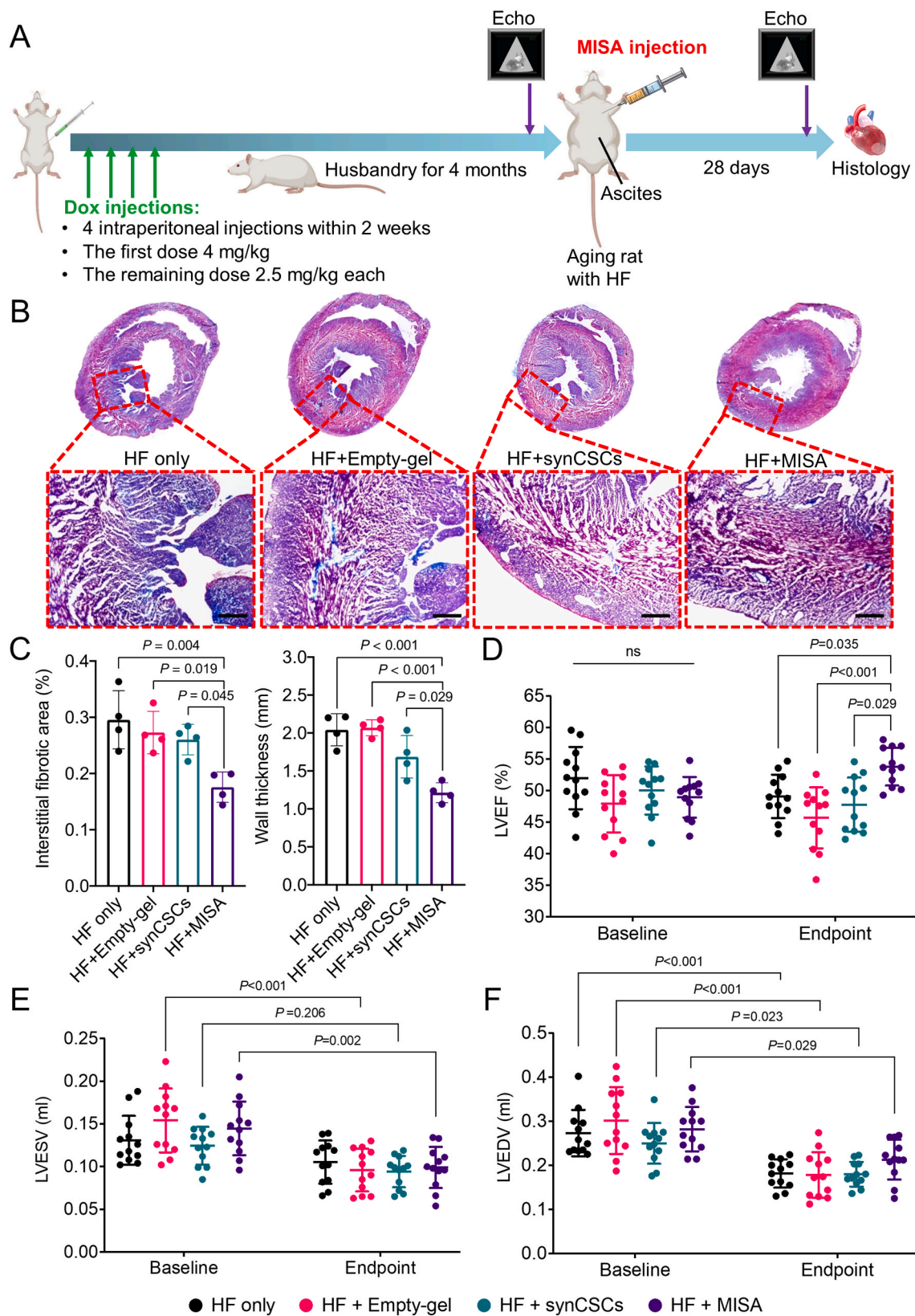
Fig. 3. Cardiac benefits in an aged rat with chemotherapy-HF after MISA treatment. A. Schematic image showing the study design. **B.** Masson's trichrome staining performed on cardiac cryosections from each group. Insets outlined by red dashed boxes are shown at higher magnification in the lower row. Scale bars, 500 μm. **C.** Morphometric parameters including interstitial fibrotic area and infarct wall thickness were measured from the Masson's trichrome–stained slides via NIH ImageJ software. n = 4 in each group. **D.** LVEF was determined at baseline (day 0) and endpoint (day 28) after HF, based on LVEDV and LVESV. n = 12 in each group. **E&F.** LVEDV and LVESV were determined at baseline (day 0) and endpoint (day 28) after HF, based on M-mode echocardiography. n = 12 in each group.

2.4. MISA mediates cardiomyocyte proliferation and angiogenesis in vivo

Histologic analyses revealed more Ki67$^+$ cardiac cells in the MISA-treated HF hearts (Fig. 4A and B). This finding was validated by pH3$^+$ nuclei found in the MISA-treated hearts (Fig. 4C and D). Furthermore, our studies revealed that MISA also improved the angiogenesis in chemotherapy-HF models, which was confirmed by the presence of more CD31$^+$ vascular endothelial cells in the MISA treatment group
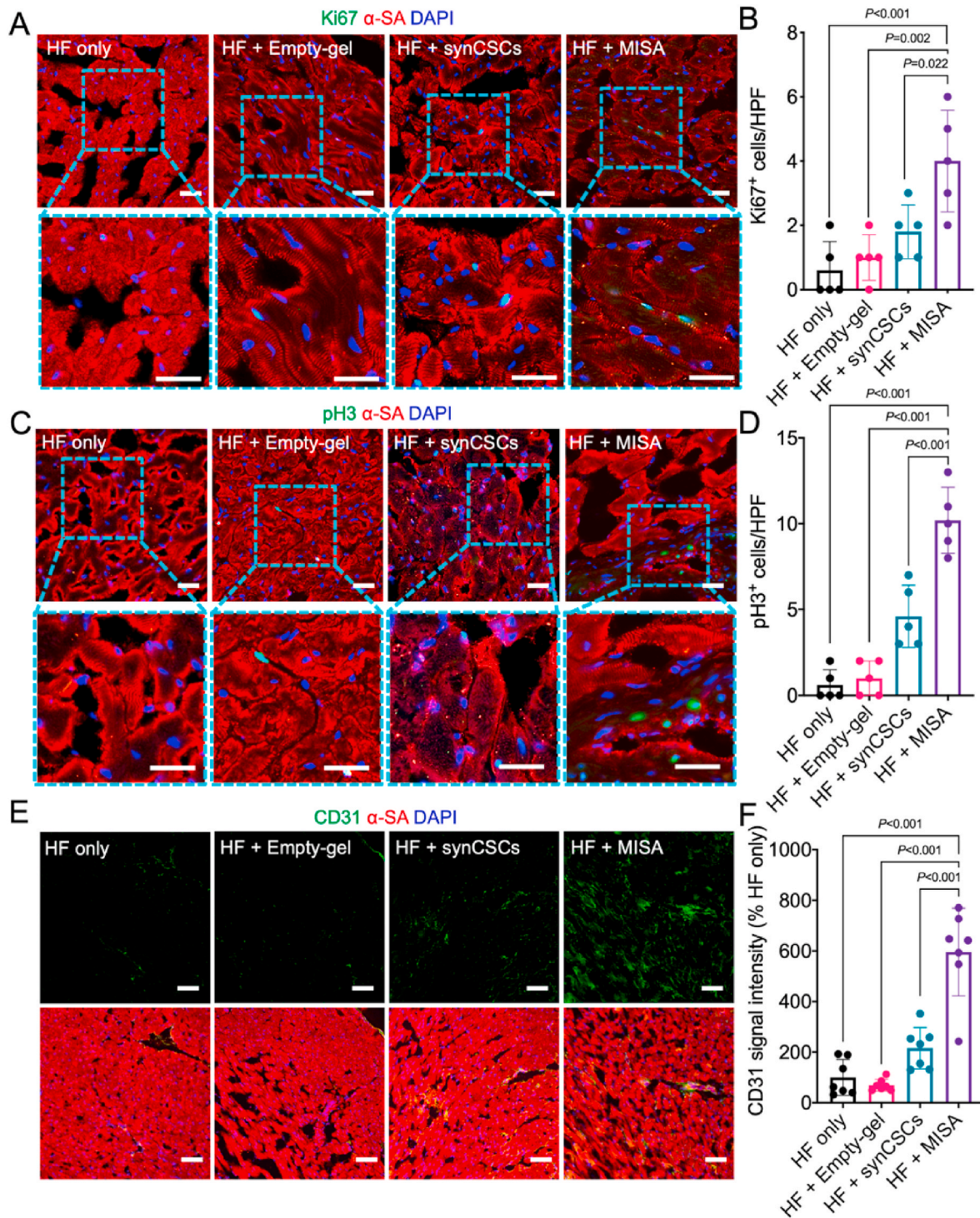

Fig. 4. Regenerative effects of MISA in the aged rat heart with HF. A. Representative images of immunofluorescence staining of Ki67 marker in CMs in different groups. Ki67 (green) was used to label proliferative cells among CMs. α-SA (red) is an indicator of CMs. Nuclei were labeled with DAPI (blue). Lower images show higher-magnification views of the boxed areas in the upper images. Scale bars, 50 μm. **B.** Quantitative analysis of cells in (**A**), n = 5 in each group. **C.** Representative images of immunofluorescence staining of pH3 marker in CMs in different groups. pH3 (green) was used to label proliferative cells among CMs. α-SA (red) is an indicator of CMs. Nuclei were labeled with DAPI (blue). Lower images show higher-magnification views of the boxed areas in the upper images. Scale bars, 50 μm. **D.** Quantitative analysis of cells in (**C**), n = 5 in each group. **E.** Representative images of immunofluorescence staining of CD31 marker in the heart in different groups. CD31 (green) was used to label vascular endothelial cells in the myocardium. α-SA (red) is an indicator of CMs. Nuclei were labeled with DAPI (blue). Upper images show green channels and lower images show merged channels. Scale bars, 50 μm. **F.** Quantitative analysis of cells in (**E**), n = 7 in each group.

compared to the control groups (Fig. 4E and F). Together, the afore-mentioned findings can explain the improvements observed in the LV function tests at the cellular level through the enhancement of cardiac proliferation and angiogenesis.

2.5. RNA sequencing illustrates the potential mechanisms of MISA-mediated cardiac repair

Heart tissues from the MISA group and the HF-only control group were harvested and were sent for bulk RNA sequencing (LC Sciences, LLC), where we listed the upregulated and downregulated genes after treatment and performed the Metascape Gene List Analysis
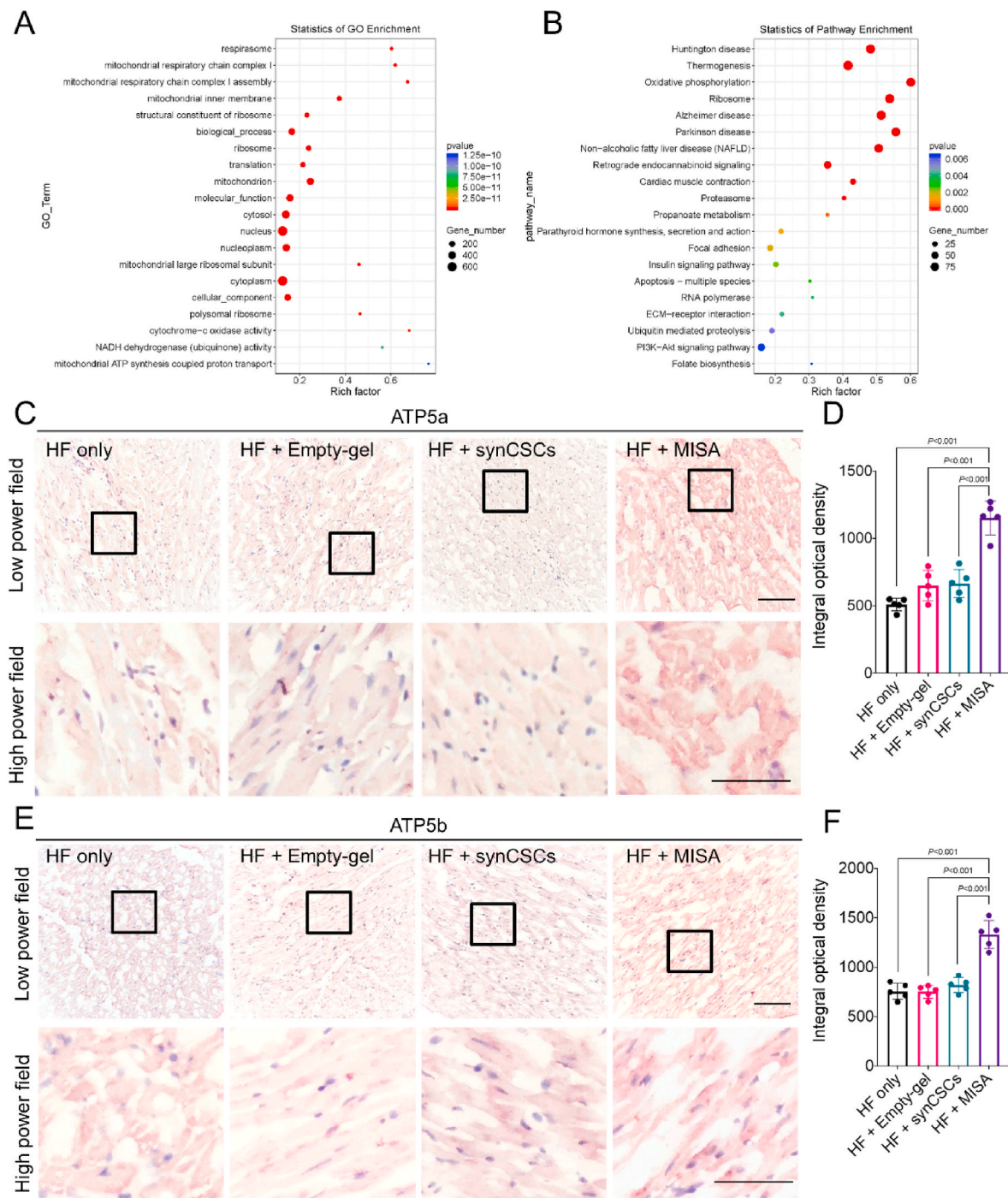
Fig. 5. MISA Improved heart mitochondrial activities. A. GO enrichment analysis of upregulated genes in heart tissues after MISA treatment. **B**. Pathway enrichment analysis of upregulated genes in heart tissues after MISA treatment. **C.** Representative images of immunohistochemistry staining of ATP5a marker (dark red) in different groups. Nuclei were labeled with hematoxylin (dark blue). Lower images show higher-magnification views of the boxed areas in the upper images. Scale bars (low power field) = 100 μm; Scale bars (high power field) = 50 μm. **D.** Quantitative analysis of integral optical density of positive signals in (**C**), n = 5 in each group. **E.** Representative images of immunohistochemistry staining of ATP5b marker (dark red) in different groups. Nuclei were labeled with hematoxylin (dark blue). Lower images show higher-magnification views of the boxed areas in the upper images. Scale bars (low power field) = 100 μm; Scale bars (high power field) = 50 μm. **F.** Quantitative analysis of integral optical density of positive signals in (**E**), n = 5 in each group.

(Figs. S5A–S5E). From GO enrichment analysis, we found that MISA led to enhanced expression of genes responsible for mitochondrial activities, including mitochondrial respiratory chain complex, mitochondrial inner membrane, mitochondrial large ribosomal subunit, and mitochondrial ATP synthesis coupled proton transport (Fig. 5A), reflecting more active mitochondria in cardiomyocytes after MISA treatment. Furthermore, the pathway enrichment analysis showed that upregulated genes in the MISA group were highly associated with oxidative phosphorylation and cardiac muscle contraction (Fig. 5B). Taken together, these data from bioinformatics collectively suggested MISA enhanced production of ATP in cardiomyocytes. To validate this observation, we utilized immunostaining to assess the expression level of protein ATP5a (ATP synthase subunit alpha) and ATP5b (ATP synthase subunit beta). Higher levels of both proteins were observed and quantified in the MISA group when compared to other groups (Fig. 5C–F). Therefore, we concluded that MISA therapy triggered more active mitochondrial respiration which leads to increased ATP synthesis and eventually resulted in stronger contractile function of the heart after chemotherapy-HF.

2.6. The safety of MISA treatment in the aged rat model of chemotherapy-induced HF

Chemistry panel analysis of the rat blood showed that the levels of albumin, total cholesterol, ALT/AST ratio, and creatinine in the MISA group were within the normal range, indicating that MISA is not only safe but also has a protective systematic effect (Figs. S6A–S6H). A potential explanation of this finding was that MISA, by improving the LV function in the HF models, preserved the kidney and liver function and offered systemically beneficial effects. Interestingly, the other control groups displayed abnormal laboratory findings indicating liver and kidney injuries most likely attributed to the chemotherapy.
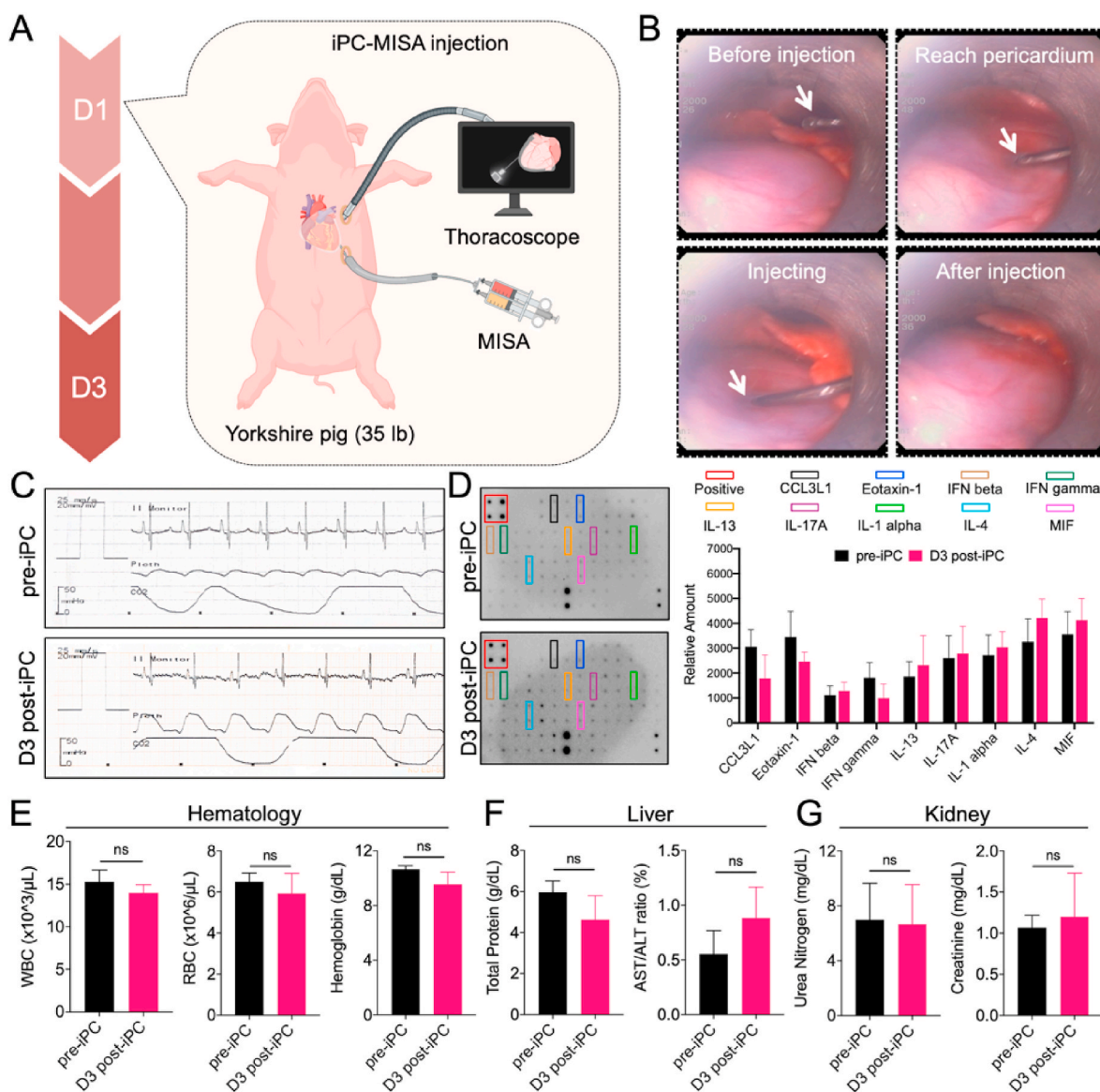
Fig. 6. Feasibility of safety of iPC-MISA injection in healthy pigs. A. Schematic image showing the video-assisted thoracoscopic iPC injection procedure in pigs. **B.** Snapshots from the thoracoscopy video showing the process of iPCinjection in pigs (Video S1). The injection needle is indicated by white arrows. **C.** Electrocardiography pre- and post-iPC injection of MISA in pig hearts. **D.** Cytokine array analysis and quantitative results of the inflammatory cytokine concentrations in pig serum pre- and post-iPC injection. No statistical significance was observed in any of these 9 cytokines between the two timepoints. n = 3. **E.** Quantitative analysis of hematologic function indices in pig serum pre- and post-iPC injection. n = 3. **F.** Quantitative analysis of liver function indices in pig serum pre- and post-iPC injection. (ALT: Alanine aminotransferase; AST: Aspartate aminotransferase). n = 3. **G.** Quantitative analysis of renal function indices in pig serum pre- and post-iPC injection. n = 3.

2.7. iPC delivery of MISA is feasible and safe in a healthy porcine model

Following the studies in our rat models, we practiced the iPC delivery of MISA in a porcine model. Three Yorkshire pigs were utilized for these experiments. MISA was injected into the pericardial space with the guidance of a thoracoscope (Fig. 6A). Briefly, two small incisions were generated on the pig's chest wall through which a sheath catheter and a thoracoscope wereintroduced into the chest cavity. The catheter was moved forward until it was in the pericardial cavity of the pig heart, while being continuously monitored thoracoscopically (Video S1). Following that, 5 ml of MISA was injected into the pericardial cavity slowly (Fig. 6B). Electrocardiography showed normal cardiac function with no abnormalities 3 days post-injection (Fig. 6C). In addition, no obvious pericardial effusions were noted. To assess the potential inflammatory response caused by MISA injection *in vivo*, 48 cytokines were quantified by densitometry and many pro-inflammatory factors among them (e.g. CCL3L1, Eotaxin-1, IFN beta, IFN gamma, IL-13, IL-17A, IL-1 alpha, IL-4, and macrophage migration inhibitory factor (MIF)) were found to have a non-significant change in the blood post-iPC compared to the pre-iPC (Fig. 6D), which showed that iPC-MISA injection did not cause a significant immune response in pigs. We also found that the blood tests, indexes of hematology, and liver and kidney function of the pigs were not significantly different after MISA injection (Fig. 6E–G). Together, iPC injection of MISA was feasible in a clinically relevant large animal model, indicating that MISA injection through an iPC procedure carries a high translative ability to clinical application.

3. Discussion

Advancements in pharmaceutical agents and left ventricular assisted devices (LVADs) have significantly improved the survival and the quality of life of patients with HF [16], however, the only definitive treatment for HF to date remains heart transplantation [6,7]. Donor hearts are in shortage and the waiting lists are long. Cancer survivors who suffer from cancer therapy-related HF are generally considered poor surgical candidates. Therefore, the likelihood of performing a heart transplantation or even an LVAD implementation procedure in these vulnerable patients is traditionally low [17], and the available treatment options are limited to medical regimens that can only offer symptomatic relief. It should also be noted that cancer patients have an already affected quality of life that can significantly deteriorate in cases where HF emerges due to cancer therapy, rendering chemotherapy-HF a very sensitive healthcare issue. For all these reasons, we believe that investigating alternative treatment modalities for this particular disease entity is a matter of paramount importance.

Utilizing cardiac stromal cells (CSCs) for heart treatment is a promising approach, and encouraging results have been reported in the current literature [18–26]. Many studies have suggested that CSCs improve cardiac function via paracrine actions [19,23] and based on these findings, synCSC had been initially developed and investigated [12,13]. These cell-mimicking microparticles have demonstrated promising cardiac benefits when injected intramyocardially or applied on the epicardial surface [12,13]. To overcome the current limitations imposed by the aggressive nature of the current chemo-induced HF treatments, we thought of utilizing the iPC injection technique to deliver this therapeutic. The iPC delivery strategy has been reported before with mixed efficacy results [27,28–34]. Our lab has showed the feasibility of the iPC route in terms of hydrogel delivery into the pericardial cavity [27,33, 35]. The notion behind using iPC as a way of therapy delivery is based on the structure of the pericardial cavity per se. The unique anatomy of the pericardium serves as a "depot" for the delivered therapeutics that further improve their retention and bioavailability making iPC a clinically applicable delivery route[36,37], especially for patients who are poor surgical candidates.

Aiming to optimize the synCSCs-based therapy, we produced MISA, an intrapericardially injectable adhesive. A major modification that was

applied in this novel therapeutic was the addition of the fibrinogen-thrombin solution in conjunction with the ECM-based gel. To outline the safety and efficacy of MISA, we tested its application in an aged rodent model of restrictive HF. To simulate the clinical thoracoscopic procedure, we delivered MISA through an endoscope-guided iPC injection. At 28 days post-treatment, MISA demonstrated significantly better therapeutic efficacy in HF rats compared to the control groups by improving LV contractility as well as reducing the myocardial fibrosis. To elucidate MISA's action, we conducted histological analysis and observed higher proliferation markers in the HF heart and we performed RNA sequencing of cardiac tissues where identified upregulated oxidative phosphorylation pathways after administration of MISA. The safety and translatability of MISA were evident also in a porcine model.

Collectively, the current MISA is an off-the-shelf minimally invasive implantable therapeutic, that can potentially overcome most of the current limitations in the treatment of chemotherapy-HF. It provides very promising results in rodent HF models and displays great translatability in porcine models. MISA also represents an "injectable organ band-aid" technology that can be applied to the creation of multiple types of synthetic cells and extracellular matrix for various organs and for different organ injuries. In addition, because MISA is ready to use and offers off-the-shelf feasibility, it can potentially be used as an acute therapy product available in the emergency department.

4. Limitations

Our mechanistic results are solely based on studies performed in small animals and therefore further evidence is needed from future high quality translational preclinical and clinical studies in order to elucidate the role of MISA in the setting of chemotherapy-HF and to clarify its indications and contraindications. Additionally, due to the stress of animal models, the survive rate remains low from baseline to endpoint. The animal models in our study may exhibit varying degrees of complications in other organs, including the liver and kidneys, which could be an uncontrollable variable. Moreover, synCSC contains a diverse array of secretomes, including proteins, miRNAs, and extracellular vesicles, among other components. It is challenging to ascertain which component is the most effective for cardiac repair. For instance, extracellular vesicles [38] can be classified by size, with exosomes being particularly noted for their robust cardiac repair capabilities of ischemic heart or non-ischemic HF [39,40], likely due to their specific miRNA and LncRNA contents [41,42,43]. However, further research is necessary to identify the most critical component for treating chemotherapy-induced HF and to elucidate the underlying protein pathways involved.

Competency in Medical Knowledge: The definitive treatment options for cancer survivors who suffer from chemotherapy-HF are very limited. Although the application of cell-derived therapeutics has been extensively studied in ischemic heart disease, little is known about the feasibility and efficacy of these novel therapeutics in the setting of chemotherapy-induced cardiotoxicity.

Translational Outlook: MISA is a minimally invasive implantable therapeutic that seems to offer beneficial effects to chemotherapy-injured myocardium. High quality translational preclinical and clinical studies are warranted in order to further elucidate the role of MISA in the setting of chemotherapy-HF.

5. Methods

5.1. Fabrication and characterization of MISA

Decellularized ECM was homogenized and lyophilized into ECM powder and sequentially enzymatically digested to create ECM gel [44, 45]. ECM-fibrinogen was created by mixing ECM gel and fibrinogen solution (1:1). SynCSCs (8×10^6/ml) were embedded into a solubilized ECM-fibrinogen solution to create the semifinal product of MISA. After concomitant injection with thrombin (10 mg/ml) via a double-lumen

syringe, the final product of MISA was formed *in situ.* More details regarding the methodology are presented in Supplementary Materials.

5.2. An aged rat model of HF

An aged rat chemotherapy-HF model was made to mimic the clinical picture of cancer patients who develop cardiotoxicity after chemotherapy administration [14]. Briefly, aged rats (one year in age) received 4 doses of DOX by intraperitoneal injection within two weeks. The first dose was 4 mg per kg of body weight and the remaining doses were 2.5 mg/kg. Subsequentially, the rats were observed for four months for the development of heart failure before any further intervention. The intrapericardial injection in our rat models was performed as previously reported [27].

More details regarding the methodology are presented in Supplementary Materials.

5.3. Statistical analysis

All experiments were performed for at least three times. Results are shown as means ± standard deviation (SD). Comparisons between two groups were performed using the two-tailed, unpaired Student's *t*-test. Comparisons between more than two groups were performed using the one-way analysis of variance (ANOVA), followed by Tukey's honestly significant difference (HSD) post hoc test. For the analysis of variance with two factors, two-way ANOVA was used and followed by Bonferroni post hoc test.

Ethics approval and consent to participate

This research was conducted in strict accordance with the recommendations outlined in the Guide for the Care and Use of Laboratory Animals of the National Institutes of Health. The experimental protocol was approved bythe Institutional Animal Care and Use Committee (IACUC) of NC State University. All personnel involved in the study received training on humane animal care and handling techniques, ensuring the well-being of the animals throughout the research process. All procedures performed in studies involving animals were in compliance with the ethical standards of the institution.

CRediT authorship contribution statement

Jialu Yao: Writing – original draft, Investigation, Formal analysis, Data curation. **Junlang Li:** Writing – original draft, Project administration, Methodology, Investigation. **Dashuai Zhu:** Validation, Software, Investigation. **Yuan Li:** Writing – review & editing, Visualization, Validation, Software. **Panagiotis Tasoudis:** Writing – original draft, Visualization, Software, Project administration. **Shuo Liu:** Writing – original draft. **Xuan Mei:** Resources, Project administration, Investigation. **Kristen Popowski:** Writing – original draft. **Thomas G. Caranasos:** Conceptualization. **Haipeng Wang:** Visualization, Methodology, Investigation. **Mingzhu Xu:** Writing – original draft, Visualization. **Tingbo Jiang:** Validation, Supervision. **Kai Shen:** Methodology, Validation. **Hongxia Li:** Supervision. **Ke Huang:** Writing – review & editing, Supervision.

Declaration of competing interest

The authors have no conflicts of interest to declare.

Acknowledgments

Appendix A. Supplementary data

Supplementary data to this article can be found online at https://doi.org/10.1016/j.bioactmat.2024.06.020.

References

[1] S.M. Bluethmann, A.B. Mariotto, J.H. Rowland, Anticipating the "silver tsunami": prevalence trajectories and Co-morbidity burden among older cancer survivors in the United States, Cancer Epidemiol. Biomarkers Prev. 25 (2016) 1029–1036.

[2] K.M. Sturgeon, L. Deng, S.M. Bluethmann, et al., A population-based study of cardiovascular disease mortality risk in US cancer patients, Eur. Heart J. 40 (2019) 3889–3897.

[3] J. Herrmann, Adverse cardiac effects of cancer therapies: cardiotoxicity and arrhythmia, Nat. Rev. Cardiol. 17 (2020) 474–502.

[4] A. Albini, G. Pennesi, F. Donatelli, R. Cammarota, S. De Flora, D.M. Noonan, Cardiotoxicity of anticancer drugs: the need for cardio-oncology and cardio-oncological prevention, J. Natl. Cancer Inst. 102 (2010) 14–25.

[5] G.H. Oliveira, M.Y. Qattan, S. Al-Kindi, S.J. Park, Advanced Heart Failure Therapies for Patients with Chemotherapy-Induced Cardiomyopathy, vol. 7, Circ Hear Fail, 2014, pp. 1050–1058.

[6] P.S. Jhund, J.J.V. McMurray, Heart failure after acute myocardial infarction a lost battle in the war on heart failure? Circulation 118 (2008) 2019–2021.

[7] M. Metra, P. Ponikowski, K. Dickstein, et al., Advanced chronic heart failure: a position statement from the study group on advanced heart failure of the heart failure association of the European society of Cardiology, Eur. J. Heart Fail. 9 (2007) 684–694.

[8] S.K. Sanganalmath, R. Bolli, Cell therapy for heart failure: a comprehensive overview of experimental and clinical studies, current challenges, and future directions, Circ. Res. 113 (2013) 810–834.

[9] M. Gyöngyösi, P.M. Haller, D.J. Blake, E. Martin Rendon, Meta-analysis of cell therapy studies in heart failure and acute myocardial infarction, Circ. Res. 123 (2018) 301–308.

[10] P. Menasché, Cell therapy trials for heart regeneration—lessons learned and future directions, Nat. Rev. Cardiol. 15 (2018) 659–671.

[11] B.A. Tompkins, W. Balkan, J. Winkler, et al., Preclinical studies of stem cell therapy for heart disease, Circ. Res. 122 (2018) 1006–1020.

[12] J. Tang, D. Shen, T.G. Caranasos, et al., Therapeutic microparticles functionalized with biomimetic cardiac stem cell membranes and secretome, Nat. Commun. 8 (2017) 13724.

[13] H.W. Ke, Oe, S. Teng, et al., An off-the-shelf artificial cardiac patch improves cardiac repair after myocardial infarction in rats and pigs, Sci. Transl. Med. 12 (2020) eaat9683.

[14] S.M. Swain, F.S. Whaley, M.S. Ewer, Congestive heart failure in patients treated with doxorubicin: a retrospective analysis of three trials, Cancer Interdiscip Int. J. Am. Cancer Soc. 97 (2003) 2869–2879.

[15] D.D. Von Hoff, M.W. Layard, P. Basa, et al., Risk factors for doxorubicin-lnduced congestive heart failure, Ann. Intern. Med. 91 (1979) 710–717.

[16] E.J. Birks, P.D. Tansley, J. Hardy, et al., Left ventricular assist device and drug therapy for the reversal of heart failure, N. Engl. J. Med. 355 (2006) 1873–1884.

[17] S.V. Deo, S.G. Al-Kindi, G.H. Oliveira, Management of advanced heart failure due to cancer therapy: the present role of mechanical circulatory support and cardiac transplantation, Curr. Treat. Options Cardiovasc. Med. 17 (2015) 1–13.

[18] T. Su, K. Huang, K.G. Mathews, et al., Cardiac stromal cell patch integrated with engineered microvessels improves recovery from myocardial infarction in rats and pigs, ACS Biomater. Sci. Eng. 6 (2020) 6309–6320.

[19] E.L. Tilokee, N. Latham, R. Jackson, et al., Paracrine engineering of human explant-derived cardiac stem cells to over-express stromal-cell derived factor 1α enhances myocardial repair, Stem Cell. 34 (2016) 1826–1835.

[20] T. Su, K. Huang, M.A. Daniele, et al., A regenerative cardiac patch formed by spray painting of biomaterials onto the heart, Tissue Eng. C Methods 23 (2017) 146–155.

[21] J. Terrovitis, R. Lautamäki, M. Bonios, et al., Noninvasive quantification and optimization of acute cell retention by in vivo positron emission tomography after intramyocardial cardiac-derived stem cell delivery, J. Am. Coll. Cardiol. 54 (2009) 1619–1626.

[22] F. Fernández-Avilés, R. Sanz-Ruiz, J. Bogaert, et al., Safety and efficacy of intracoronary infusion of allogeneic human cardiac stem cells in patients with ST-segment elevation myocardial infarction and left ventricular dysfunction: a multicenter randomized, double-blind, and placebo-controlled tria, Circ. Res. 123 (2018) 579–589.

[23] N. Latham, B. Ye, R. Jackson, et al., Human blood and cardiac stem cells synergize to enhance cardiac repair when cotransplanted into ischemic myocardium, Circulation 128 (2013) S105–S112.

[24] J. Tang, X. Cui, T.G. Caranasos, et al., Heart repair using nanogel-encapsulated human cardiac stem cells in mice and pigs with myocardial infarction, ACS Nano 11 (2017) 9738–9749.

[25] R. Bolli, X.-L. Tang, S.K. Sanganalmath, et al., Intracoronary delivery of autologous cardiac stem cells improves cardiac function in a porcine model of chronic ischemic cardiomyopathy, Circulation 128 (2013) 122–131.

[26] J. Tang, T. Su, K. Huang, et al., Targeted repair of heart injury by stem cells fused with platelet nanovesicles, Nat. Biomed. Eng. 2 (2018) 17–26.

[27] D. Zhu, Z. Li, K. Huang, T.G. Caranasos, J.S. Rossi, K. Cheng, Minimally invasive delivery of therapeutic agents by hydrogel injection into the pericardial cavity for cardiac repair, Nat. Commun. 12 (2021) 1412.

[28] J. Li, S. Hu, D. Zhu, et al., All roads lead to Rome (the heart): cell retention and outcomes from various delivery routes of cell therapy products to the heart, J. Am. Heart Assoc. 10 (2021) e020402.

[29] D. Ladage, I.C. Turnbull, K. Ishikawa, et al., Delivery of gelfoam-enabled cells and vectors into the pericardial space using a percutaneous approach in a porcine model, Gene Ther. 18 (2011) 979–985.

[30] T.M. Kolettis, N. Kazakos, C.S. Katsouras, et al., Intrapericardial drug delivery: pharmacologic properties and long-term safety in swine, Int. J. Cardiol. 99 (2005) 415–421.

[31] R.J. Laham, M. Rezaee, M. Post, et al., Intrapericardial delivery of fibroblast growth factor-2 induces neovascularization in a porcine model of chronic myocardial ischemia, J. Pharmacol. Exp. Therapeut. 292 (2000) 795 LP–802.

[32] R. Blázquez, F.M. Sánchez-Margallo, V. Crisóstomo, et al., Intrapericardial delivery of cardiosphere-derived cells: an immunological study in a clinically relevant large animal model, PLoS One 11 (2016) e0149001.

[33] J. Li, Y. Lv, D. Zhu, et al., Intrapericardial hydrogel injection generates high cell retention and augments therapeutic effects of mesenchymal stem cells in myocardial infarction, Chem. Eng. J. 427 (2022) 131581.

[34] R. Gj, F. Cp, K. Gautam, et al., A minimally invasive, translational method to deliver hydrogels to the heart through the pericardial space, JACC Bas. Transl. Sci. 2 (2017) 601–609.

[35] Z. Li, D. Zhu, Q. Hui, et al., Injection of ROS-responsive hydrogel loaded with basic fibroblast growth factor into the pericardial cavity for heart repair, Adv. Funct. Mater. (2021) 2004377.

[36] D. Zhu, S. Liu, K. Huang, J. Li, X. Mei, Z. Li, K. Cheng, Intrapericardial long non-coding RNA–Tcf21 antisense RNA inducing demethylation administration promotes cardiac repair, Eur. Heart J. (2023) ehad114.

[37] D. Zhu, S. Liu, K. Huang, Z. Wang, S. Hu, J. Li, Z. Li, K. Cheng, Intrapericardial Exosome Therapy Dampens Cardiac Injury via Activating Foxo3, Circ. Res. 131 (2022) e135–e150. https://doi.org/10.1161/CIRCRESAHA.122.321384.

[38] K. Cheng, R. Kalluri, Guidelines for clinical translation and commercialization of extracellular vesicles and exosomes based therapeutics, Extracell. Vesicle 2 (2023) 100029.

[39] R. Vaka, S Van Remortel, V. Ly, D.R. Davis, Extracellular vesicle therapy for non-ischemic heart failure: a systematic review of preclinical studies, Extracell. Vesicle 1 (2022) 100009.

[40] X. Chen, L. Zhu, J. Liu, Y. Lu, L. Pan, J. Xiao, Greasing wheels of cell-free therapies for cardiovascular diseases: integrated devices of exosomes/exosome-like nanovectors with bioinspired materials, Extracell. Vesicle 1 (2022) 100010.

[41] M. Spanos, P. Gokulnath, E. Chatterjee, G. Li, D. Varrias, S. Das, Expanding the horizon of EV-RNAs: LncRNAs in EVs as biomarkers for disease pathways, Extracell. Vesicle 2 (2023) 100025.

[42] Z. Ding, Z.F. Greenberg, M.F. Serafim, et al., Understanding molecular characteristics of extracellular vesicles derived from different types of mesenchymal stem cells for therapeutic translation, Extracell. Vesicle 3 (2024) 100034.

[43] E. Tzng, N. Bayardo, P.C. Yang, Current challenges surrounding exosome treatments, Extracell. Vesicle 2 (2023) 100023.

[44] S.B. Seif-Naraghi, J.M. Singelyn, M.A. Salvatore, et al., Safety and efficacy of an injectable extracellular matrix hydrogel for treating myocardial infarction, Sci. Transl. Med. 5 (2013), 173ra25-173ra25.

[45] J.M. Singelyn, J.A. DeQuach, S.B. Seif-Naraghi, R.B. Littlefield, P.J. Schup-Magoffin, K.L. Christman, Naturally derived myocardial matrix as an injectable scaffold for cardiac tissue engineering, Biomaterials 30 (2009) 5409–5416.